BILINGUAL PUBLISHING CO.
Pioneer of Global Academics Since 1984

Journal of Mechanical Materials and Mechanics Research
https://ojs.bilpublishing.com/index.php/jmmmr

ARTICLE

Thermo-Mechanical Analysis of a Typical Vehicle Engine Using PTC-Creo

Jafar Mahmoudi*

Department of Sustainable Production Development, School of Industrial Engineering and Management, KTH Royal Institute of Technology, Stockholm, Sweden

ARTICLE INFO

Article history
Received: 20 April 2022
Revised: 20 September 2022
Accepted: 5 November 2022
Published Online: 29 November 2022

Keywords:
Stress analysis
Engine failure
PTC-Creo
Thermomechanical analysis

ABSTRACT

In this work, a typical vehicle engine is modeled within PTC-Creo software, and its thermal, mechanical, and thermo-mechanical performance are evaluated. This is followed by the vibrational, fatigue, and buckling analysis of the assembly of components, which are the predominant failure causes. The results show that the least temperature gradient occurs in the center of the pin, which connects the piston to the connecting rod, the maximum displacement is seen just below the piston head, and the thermo-mechanical failure is caused mostly (about 85%) by the mechanical load rather than the thermal one. Also, in fatigue analysis, the minimum and maximum values for the safety factor are 0.63 and 5, respectively. The results can prevent the reoccurrence of similar failures and help the enhancement of the components' design and manufacturing process.

1. Introduction

As a power-producer component, the engine has a fundamental and crucial role in vehicles. Analysis of the factors affecting the engine's performance is very important, which should be accompanied by the identification of defects and failures in its components. The major components of an engine are the piston, connecting rod, and crankshaft [1].

The connecting rod transforms the reciprocating motion of the piston into the rotational movement of the crankshaft. These components have relatively complex manufacturing processes and procedures [2], and thus their proper design and analysis are of high importance before manufacturing, which can prevent the reoccurrence of similar failures [3]. For this purpose, it is imperative to investigate the performance of crucial components under the mechanical and thermal loads along with the consideration of the main potential failures, such as the fatigue failure.

To analyze the performance of an engine's components under different loading scenarios and their possible failures, both experimental and numerical methods are used. While the former approach is valuable, it entails spending high costs in comparison with the latter approach. Among numerical methods, the Finite Element Method (FEM) is a well-established procedure which has a high

*Corresponding Author:
Jafar Mahmoudi,
Department of Sustainable Production Development, School of Industrial Engineering and Management, KTH Royal Institute of Technology, Stockholm, Sweden;
Email: Mahmoudi@kth.se

DOI: https://doi.org/10.30564/jmmmr.v5i2.4600

simulation capability. Different software such ANSYS, CATIA, MSC/Nastran are utilized in this regard [4,5]. Note that Computer-Aided Design (CAD) is obviously the key component of computerized mechanical engineering. The incorrect or corrupted CAD model causes many problems in Computer-Aided Manufacturing (CAM) and Computer-Aided Engineering (CAE) applications. Typical vehicle main components are given here (Figure 1).

Figure 1. Individual components of the assembly, including piston, connecting rod, pin, and crankshaft

Considering the above explanations, numerous research works have been done on the engine, especially on the crucial components, including piston, connecting rod, and crankshaft. Liu et al. [6] investigated the piston of a diesel engine in different thermal, mechanical, and thermal-mechanical coupling conditions using FEM. Zhaoju et al. [7] calculated the temperature field distribution of a diesel engine piston in static compression state and the thermo-mechanical coupling stress.

The comparisons showed that the mechanical load is the major stress. Gopi et al. [8] determined the structural and thermal stress distribution of piston rings using CATIA and ANSYS. Rajakumar and Karthiyaraj [9] examined the piston's structural and thermal response using FEM method. They compared the results for aluminum alloy, carbon graphite, and tungsten and concluded that either carbon graphite or tungsten can be used instead of aluminum alloy. Another recent work on the piston is done by Deulgaonkar et al. [2], who carried out Failure Mode and Effect Analysis (FMEA) to provide a deeper understanding of the piston failure along with the usage of experimental methods, including Scanning Electron Microscopy (SEM), Energy Dispersive Spectrometry (EDS) and X-Ray Diffraction (XRD).

On the connecting rod, Strozzi et al. [10] examined the potential failures by dividing it into three parts, including the shank, the small and the big ends. Anderson and Yukioka [11] provided the buckling analysis using two primary FEM methods, namely, the eigenvalue and explicit dynamics. Muhammad and Shanono [12] did the static analysis and weight optimization of a connecting rod and recommended the usage of ANSYS software in production companies. Also, some of the reasons for the failure of the connecting rod are mentioned as overloading, bearing failing, uneven changes of the screws as well as faulty setting up or fatigue. Pani et al. [13] evaluated the buckling strength of a connecting rod suffering from hydro-lock failure. They estimated the critical buckling stress using the Merchant-Rankine and slider-crank approaches and resulted that suitable Buckling Safety Factor (BSF) should be regarded based on the maximum buckling stress to avoid such failures. Rezvani et al. [14] analyzed the connecting rod of a failed locomotive engine using a theoretical procedure, experimental modal testing, and FEM-based simulation. They found the natural frequencies and mode shapes of the component and calculated the critical buckling forces. Witek and Zelek [15] performed the failure analysis of the connecting rod of a turbocharged diesel engine using CATIA for geometrical modeling and ANSYS for stress analysis. Andoko et al. [16] also demonstrated that the values of stress and strain are larger in the area near the big end of the connecting rod.

Analysis of crankshafts is also widely carried out in the literature. Rodrigues et al. [17] presented the modal analysis of a six-cylinder crankshaft using both numerical and experimental approaches. Based on the resulted mode shapes and natural frequencies, damping factors were estimated to be used in dynamic analysis. Ang and Ku [18] used SolidWorks and ANSYS for the fatigue and modal analysis of an automotive crankshaft. Kumar et al. [19] analyzed the crankpin failure in a single-cylinder engine. They introduced some potential reasons for the failure of crankshaft assembly and crankpin as, for example, shaft misalignment, improper lubrication, vibration ensued of the bearings, and based on their results, the lower surface hardness was known as the main reason of failure. The paper mentioned the crankpin fillet as the most critical area of the crankshaft [20]. A similar conclusion is stated for the crankshaft of a helicopter engine [21]. Gomes et al. [22] investigated the seven cases of crankshaft's failures in marine diesel engines and listed some of the failure causes, followed by the proposition of some design modifications. Jiao et al. [23] did the modal and fatigue analysis of a crankshaft in addition to the physical and chemical scrutiny and introduced the main cause of crankshaft failure as fatigue resulted from overload. Kubet et al. [24] provided the static, modal, and harmonic analyses. The latter is used to determine the harmful frequencies of vibrations, having the possibility to break the structure.

While the above-mentioned references have made valuable contributions, the present work aims to provide three main contributions: (1) simultaneous analyses of thermal, mechanical, and thermomechanical in an assembly of components, without the dependent analysis of components, as done in most of the given references, (2) consideration of three important failure mechanisms, including the vibration, fatigue, and buckling, being the main failure causes, and (3) using PTC-Creo as both CAD and CAE software that helps to prevent the possible problems of using two different CAD and CAE software. Also, the utilized software has been used in limited works so far [25-27], or used solely as a CAD tool, such as its usage along with ANSYS in reference [25]. For this purpose, initially, the procedure for thermal, mechanical, and thermomechanical analyses is explained. Then, the modal analysis is described, followed by the investigation of two failure mechanisms, i.e., fatigue and buckling. Finally, the results and discussions are provided in Section 4.

2. Modeling

In this section, we provide the CAD modeling and FEA analyses. In this work, CAD and CAE Creo v5.0.2

environments are employed for the physical modeling and simulation of a typical engine. PTC-Creo offers integrated environments for CAD, CAM, and CAE and reduces data losing through the CAD transferring to the CAE tools.

The first step in FEA simulation is to create an accurate CAD file. The assumed system consists of the assembly of the piston, the connecting rod, the pin between the piston and concocting rod, and the crankshaft. The individual 3D models are shown in Figure 2, and the assembly model is illustrated in Figure 3.

The second step is the material assignment. In our analysis, steel is chosen for the crankshaft, and aluminum is used for piston, connecting rod, and pin [28]. The material choice of the components is addressed in several research works [24,29]. Generally, accurate material behavior depends on the strain rate, temperature, material texture, and so on. In this work, some assumptions are considered to simplify this behavior.

The material is supposed to be isotropic with a linear stress-strain response to the forces, and two different failure formulations are selected to discuss. Hence, the material assignment is applied according to Table 1 for aluminum and Table 2 for steel. Typical mechanical properties and the governing equations are given in Figure 4.

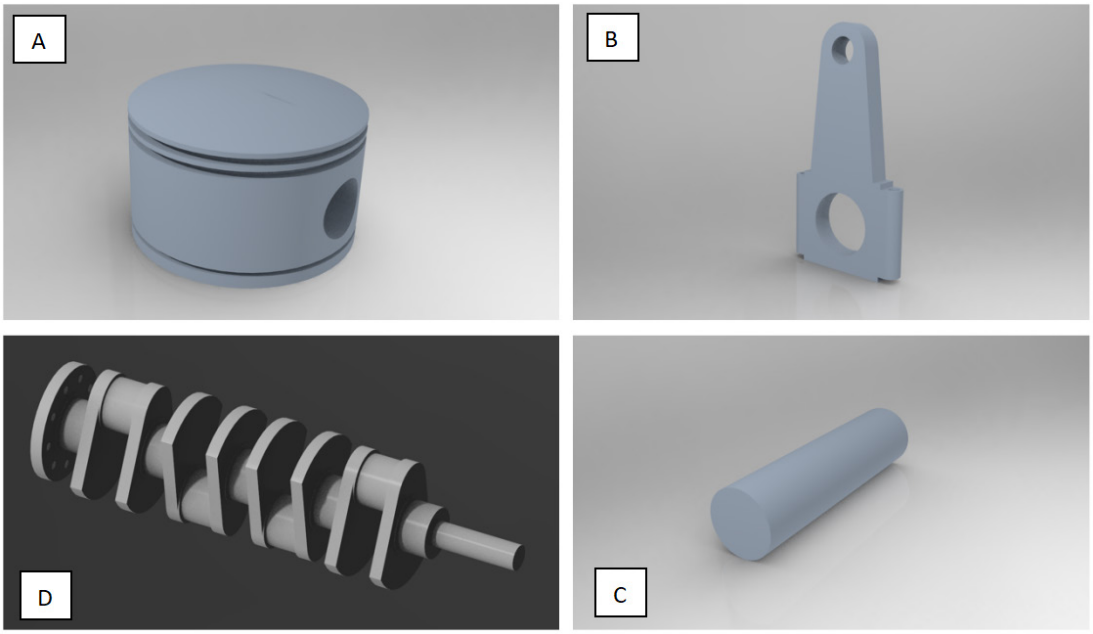

Figure 2. Simulation domain of individual components of the assembly, including A) piston, B) connecting rod, C) pin, and d) crankshaft

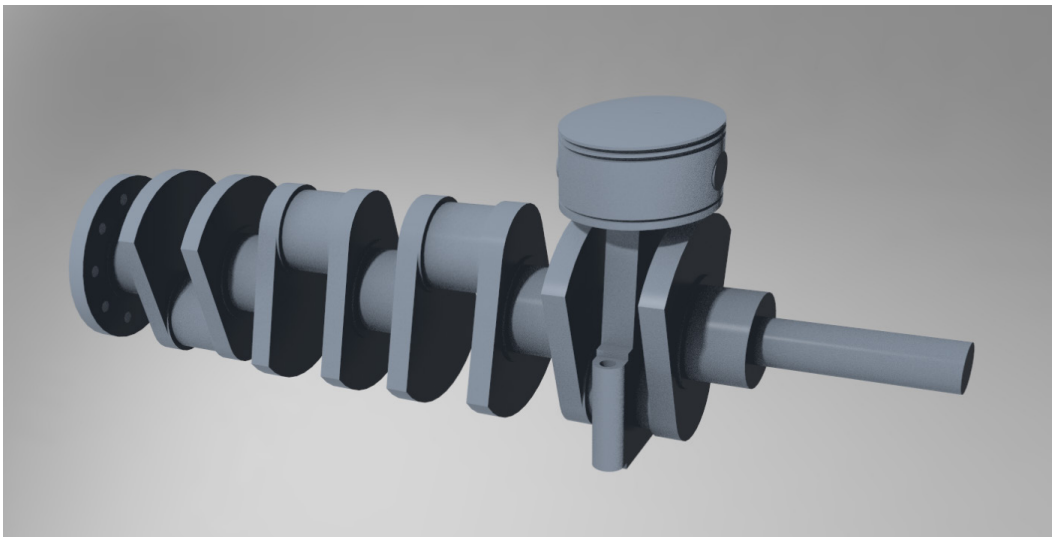

Figure 3. Simulation domain of the aassembly of the components

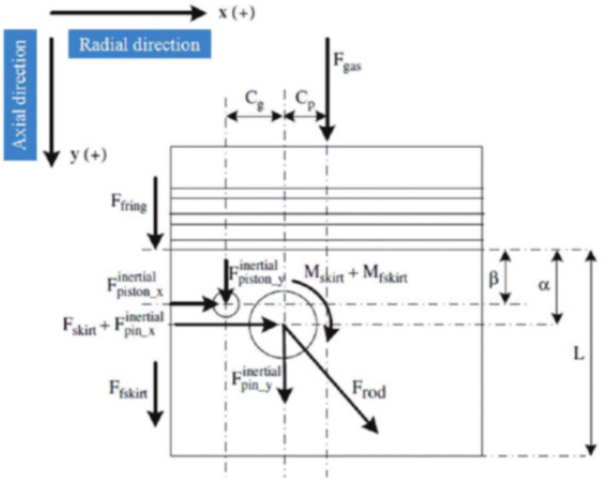

$$\sum F_y = F_{gas} + F_{f\,ring} + F_{f\,skirt} + F_{inertial\ pin\_y} + F_{inertial\ piston\_y} + F_{rod}\cos\theta = 0$$

$$\sum F_x = F_{skirt} + F_{inertial\ pin\_x} + F_{inertial\ piston\_x} - F_{rod}\cos\theta = 0$$

$$\sum M = M_{skirt} + M_{inertial\ piston} + M_{inertial\ piston\_x}(\alpha - \beta) + F_{inertial\ piston\_y}C_g + F_{gas}C_p + F_{f\,ring}C_p + M_{fskirt} + M_{f\,pin} = 0$$

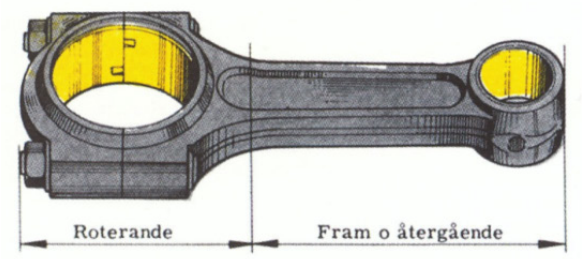

Material	Density $\rho[kg.m^{-3}]$	Stiffness E [GPa]	Yield stress $\sigma_y[MPa]$	Specific strength $[MPa.m^3/tn]$
Steel 300M	8000	205	1586	198
Aluminium T6	2800	75	413	148
Titanium alloy	4500	115	1000	222
CF weave	1600	70	600	375
CF UD	1600	135	1300	813

Figure 4. Typical mechanical properties and the governing equationas used in this study.

Table 1. Material properties of wrought Aluminum [30]

Specification	Value	Unit
Poisson's ratio	0.33	-
Young's Modulus	7.05e+07	KPa
Thermal expansion coefficient	2.35e-05	1/ºC
Specific heat capacity	8.98e+08	$mm^2/(s^2ºC)$
Thermal conductivity	229000	$mm\ kg/(s^3ºC)$
Density	2.71e-06	kg/mm^3
Tensile ultimate strength	290	MPa
Tensile yield strength	185	MPa

Table 2. Material properties of steel [30]

Specification	Value	Unit
Poisson's ratio	0.28	-
Young's Modulus	2e+08	KPa
Thermal expansion coefficient	9.95e-06	1/ºC
Specific heat capacity	4.74e+08	$mm^2/(s^2ºC)$
Thermal conductivity	24900	$mm\ kg/(s^3ºC)$
Density	7.75e-06	kg/mm^3
Tensile ultimate strength	500	MPa
Tensile yield strength	350	MPa

The third step is defining the type of analysis. All of the contact areas between the components are assumed as bounded. This means the non-linearity is neglected due to simplification. In this work, thermal, mechanical, thermo-mechanical, fatigue, buckling, and frequency analyses are discussed. Then, the related boundary conditions and loads are specified.

For the thermal analysis, using the convection coefficient of the utilized metals, boundary conditions are considered for their free contact with the air. Table 3 shows the related values. Also, the power consumption of the engine is assumed about 1000 watts.

Table 3. Boundary conditions of the thermal simulation

Part Name	Value	Material
Convection coefficient of piston	250 $watt/m^2c^2$	Al
Convection coefficient of pin	270 $watt/m^2c^2$	Al
Convection coefficient of connecting rod	200 $watt/m^2c^2$	Al
Crankshaft	100 $watt/m^2c^2$	Steel
Reference temperature	25 °C	-
Head load on piston head	1000 Watt	-

For the mechanical analysis, it is supposed that two forces, i.e., a 6 MPA load on the piston head combined with gravity, apply to the whole assembly. Table 4 showed the boundary condition of the simulation [28]. As Figures 4-5 show, both rotational and transitional freedoms are constrained from the end and start of the crankshaft. In

this study, the failure index is also measured as a function of Tresca criteria.

Table 4. Boundary conditions of mechanical simulation

Specification	Value	Unit
Load	104	Kg
Heat transfer coefficient	17	W/m^2*K
Reference temperature	25	°C
Mechanical load	6	MPa
Gravitational acceleration	9.8	m/s^2

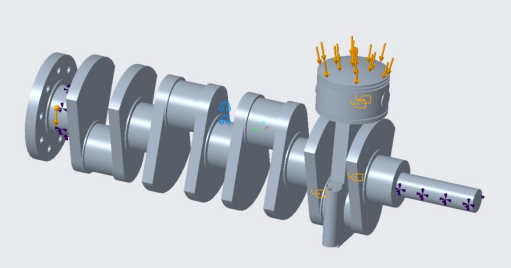

Figure 5. The mechanical analysis boundary condition

The third simulation is the thermomechanical analysis, considering the mechanical load and the thermal load of the first simulation simultaneously. All of the boundary and material conditions are the same as the previous related tables (Tables 3-4).

In order to find the damping time of the system, a dynamic study is required. Because of the superiority of modal analysis to dynamic simulation in PTC-Creo and to get some information about the resonance frequencies, firstly, modal analysis is provided. Table 5 shows frequencies and corresponsive mode shape numbers. While each mode shape and resonance frequency have their importance, the first mode shape is the lowest and thus the critical one. After modal analysis, dynamic simulation is used to find the stress variation with respect to time considering a certain damping ratio.

Table 5. Frequencies and corresponsive mode shape number

Mode shape No.	Frequency
Modes shape 1	276.993 Hz
Modes shape 2	452.868 Hz
Modes shape 3	547.086 Hz
Modes shape 4	608.385 Hz

The next step is the important fatigue analysis, which is described as the cause of most crankshafts' failures in a recent review paper by Jiregna et al. [31]. It examines the susceptibility of the model to fatigue damage when subjected to a varying load. In this study, the stress cycles are assumed regular because of the constant speed of the crankshaft. Hence, constant amplitude loading is employed. Firstly, a static analysis is carried out, and the resulted stresses are multiplied by the load factors, chosen from the range of zero to one. Materials are assumed isotropic with the same properties as Tables 3-4.

The fatigue properties are derived from the Uniform Material Law (UML), proposed by Baumel & Seeger [32] to estimate the fatigue life of aluminum and titanium alloys and extended to high-strength steels [33]. The surface of all components is assumed as well-finished, and the failure strength reduction factor is used to reduce the endurance limit. It takes into account for un-modeled stress concentrations, supposed as 1. Also, the desired endurance is envisioned.

Finally, an investigation of buckling is followed. Creo Simulate determines a buckling load factor (BLF) and the corresponding mode form for each case of buckling. It gives the BLF values using two methods. Next, a static study is needed in which Creo measures the model's pressure stiffness due to the applied forces. After that, according to the geometry and product properties, buckling analysis is used to determine the elastic strength of the prototype. Such an examination is a linear bifurcation instability analysis of its value [34]. Large displacement or non-linear buckling investigations may yield significantly different results, depending on the model type and loads being examined.

3. Results and Discussion

In this section, the results of the above-mentioned analyses are provided in the same order as Section 2. For the thermal analysis, the temperature distribution and gradient are shown in Figure 6.

As seen in this figure, the maximum temperature is about 396 °K. Also, the least temperature gradient is in the center of the pin, which connects the piston to the connecting rod. Similar results on the thermal analysis are reported [35]. For the mechanical analysis, Figure 7 (a and b) shows the Von-Mises stress distribution of the assembly after applying the loads. Most of the stress concentration is focused on the sharp corners, which is about 2.94 KPa. It is seen that the maximum value of this factor is around 1.8, concentrated in the sharp corners of the crankshaft. Displacement distribution is also shown in Figure 8. As expected, maximum displacement occurs just below the piston head and is about 0.94 mm.

For the thermomechanical analysis, Figure 9a indicates the displacement distribution. Maximum displacement occurs on the head of the piston, which is about 1 mm. Figures 9b and cc show the Von-mises stress and Tresca failure index distribution, respectively. It is clear that the maximum stress is about 2.91 KPa, the maximum failure

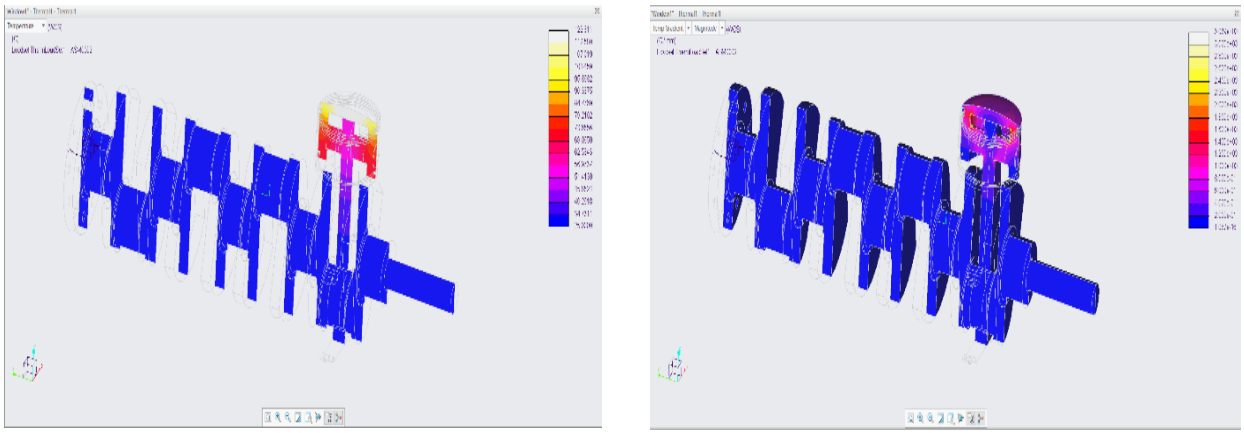

a) b)

Figure 6. Thermal analysis: (a) Temperature distribution on the half-transparent model, and (b) temperature gradient

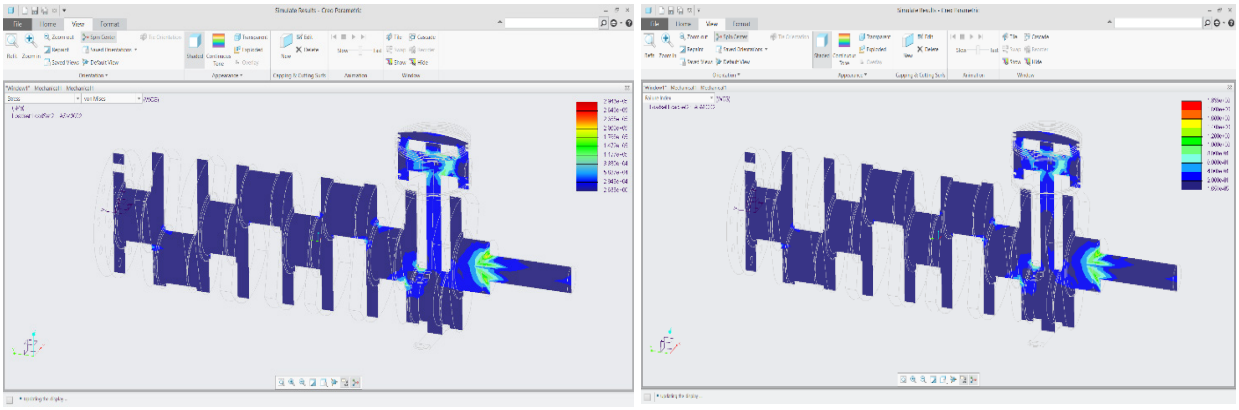

a) b)

Figure 7. Mechanical analysis: (a) Von-Mises stress distribution, and (b) Tresca failure index distribution

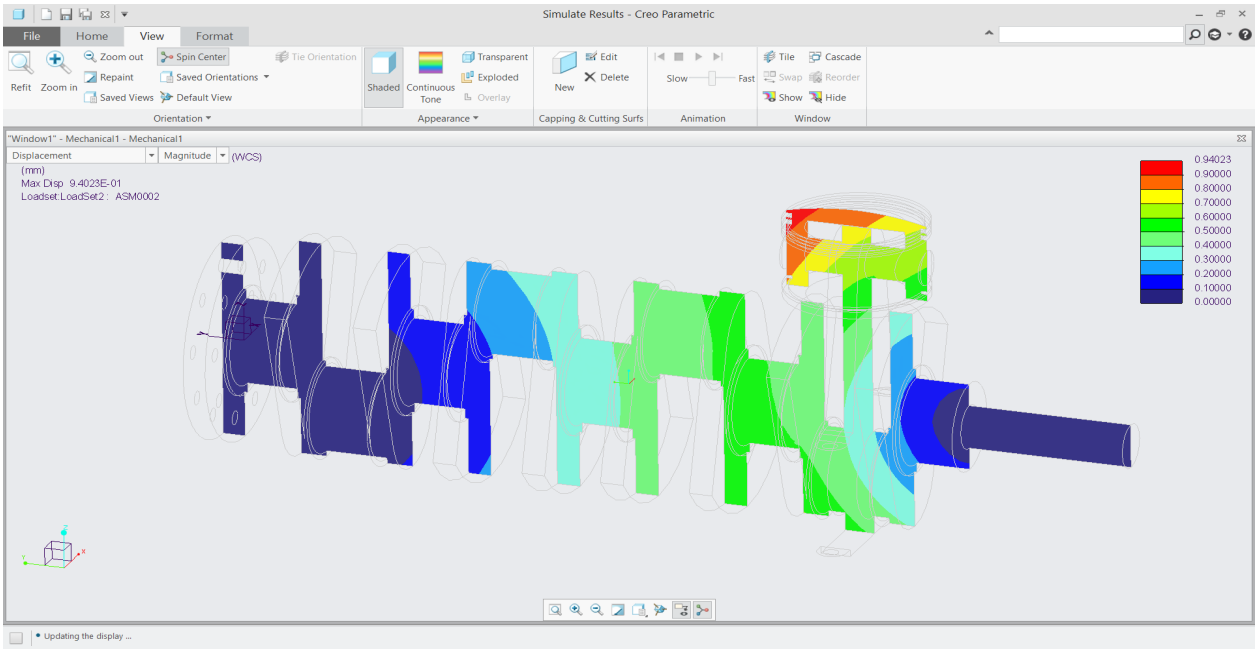

Figure 8. Displacement distribution of mechanical analysis

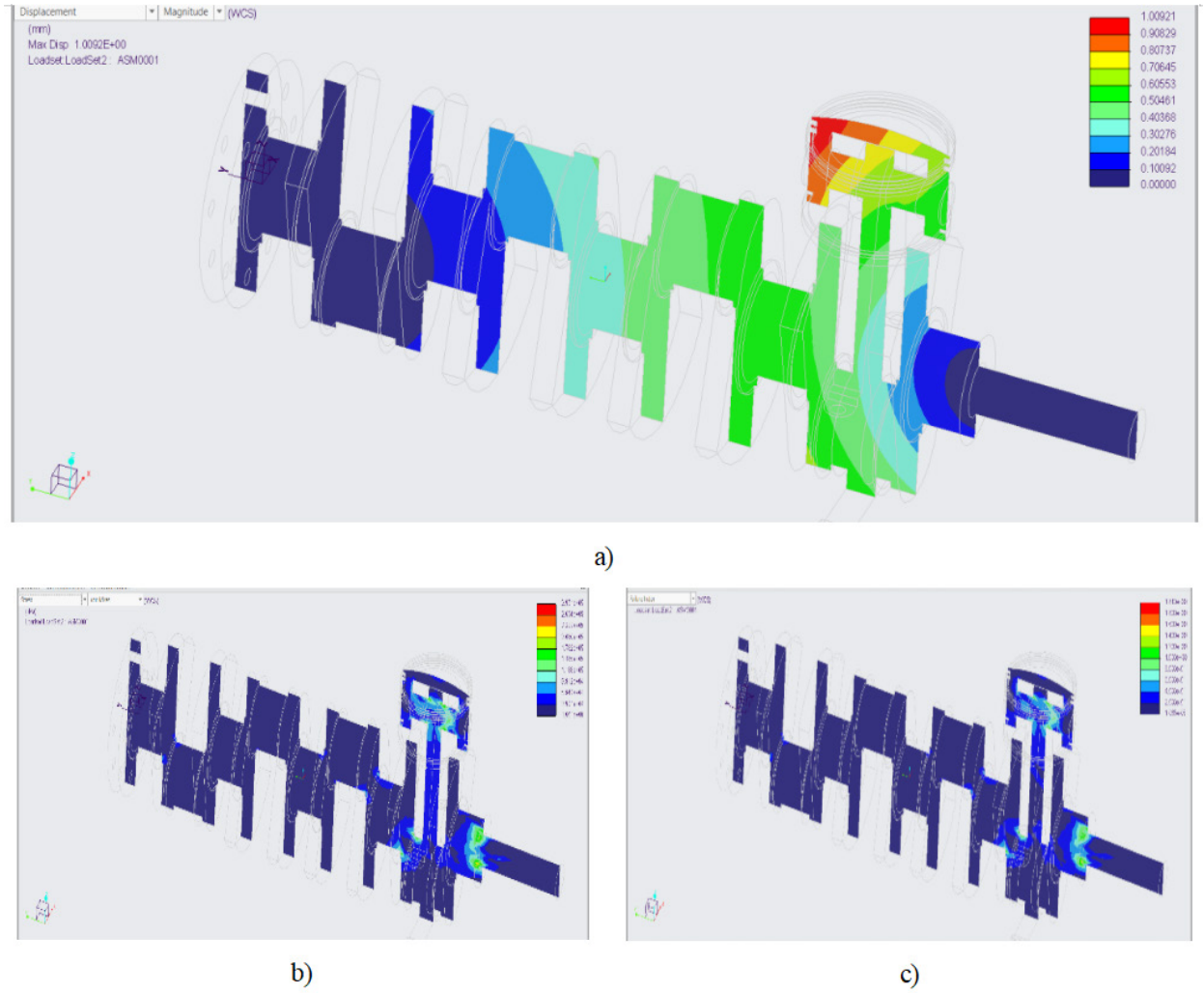

Figure 9. Thermomechanical analysis: (a) Displacement distribution of the thermomechanical simulation, (b) Von-mises stress thermomechanical simulation, and (c) Tresca Failure Index Thermomechanical

index (minimum safety factor) is about 1.8, and both of them are located in sharp corners. Similar results are reported [6] for the displacement and stress analysis of the connecting rod.

Figure 8 shows the mode shapes of 1 to 4, respectively. Figure 10 represents the dynamic response history. In this figure, the vertical axis is stress, and the horizontal axis is time. Visibly, the maximum stress happens after approximately 0.001 seconds and with damping ratio 39%, it goes steady on 0.004 seconds. From the modal analysis, it is clear that there are some resonance frequencies from 276 Hz to 608 Hz (Table 5). The rotation per minute of the crankshaft could be different and must be simulated for different speeds. Although it is not sometimes possible to avoid the resonance, the designer must therefore apply a particular procedure, for example, fast-changing of crankshaft's RPM when it comes to the resonance speed.

Results of fatigue analysis are provided in Figure 12 show the thermo-mechanicals analyse of different components in general assembly, and it is the ratio of the accumulated fatigue cycles and the total number of cycles to failure. Failure is indicated by a value greater than one. For example, a value of 0.5 represents a loss of 50% in the model's useful life. Due to the exponential nature of fatigue, expressing the ratio of damage in a logarithmic form is useful. Accumulated cycles of fatigue are the number of periods that the system encounters before the study of fatigue is carried out. Figure 10b shows the logarithm of life, and it estimates the number of cycles until the model breaks. In this case, the grey color is 10^{20}, and the red is 10^{4} number of cycles.

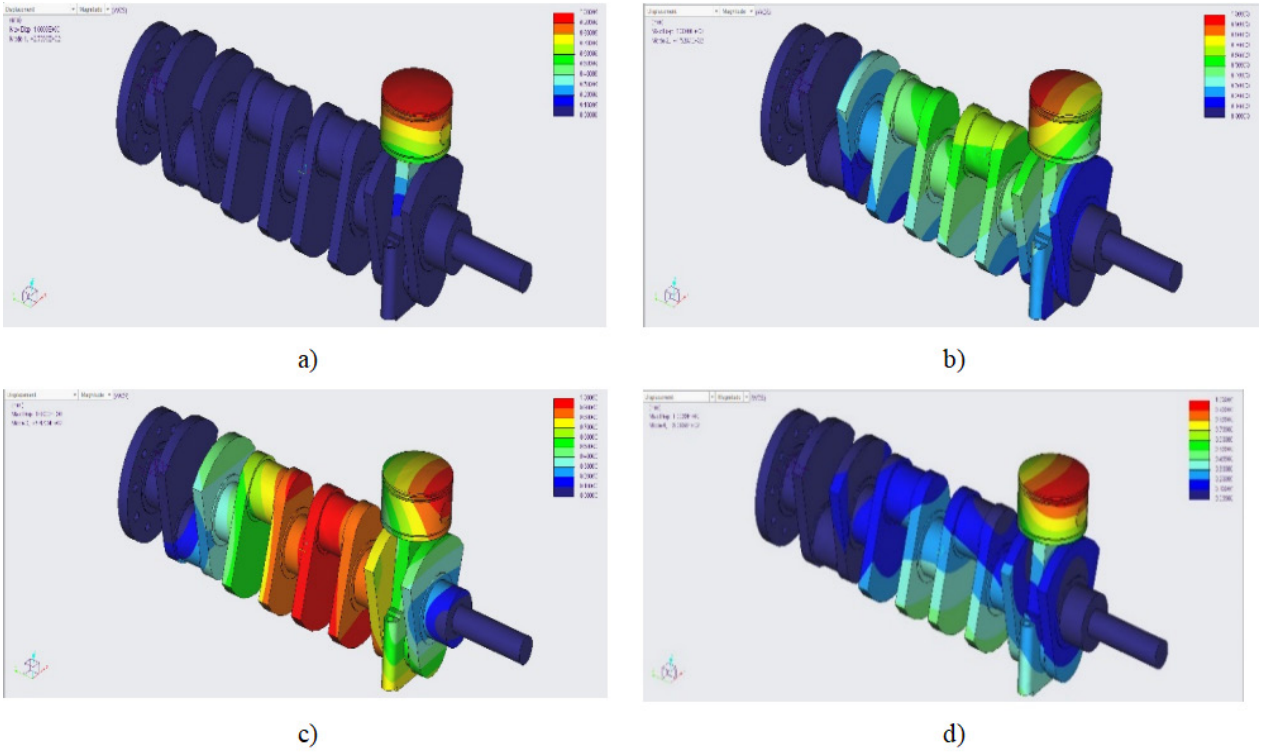

Figure 10. Modal analysis: (a) mode shape 1, (b) mode shape 2, (c) mode shape 3, and (d) mode shape 4.

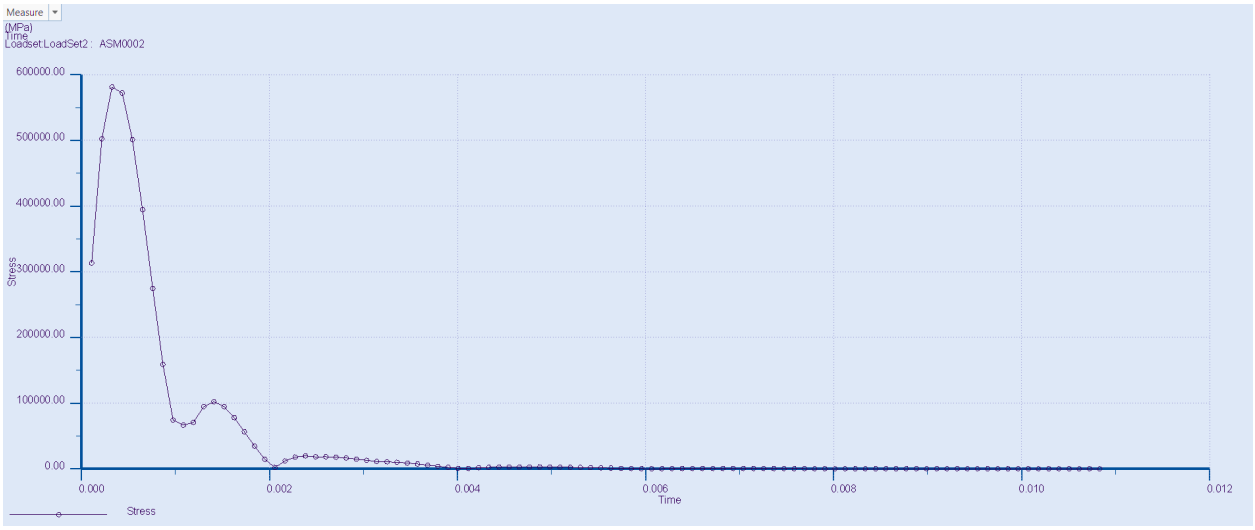

Figure 11. Time vs. Stress Dynamic Time

Figure 13 shows the thermo- mechanicals analyse of the connecting rod.

In PTC-Creo simulation, when the fatigue life calculated for the model is greater than the target design life, the software carries out a back-calculation to determine a permissible SF on the input load. As Figure 10c illustrates, 0.63 and 5 are the minimum and maximum values for the SF in fatigue analysis, respectively. Again, the sharp corners have absorbed the failure.

Figure 14 shows the confidence of life, which is the ratio of the calculated life to the targeted design life, i.e., the desired endurance. Values below one show failure, and those above three usually reflect a reasonable trust to achieve the desired target. The software displays life confidence resulting in a tri-colored fringe to provide an overview of where the model breaks first and the model endures more cycles. Red means life confidence from 0 cycles to the number of cycles obtained for optimal endur-

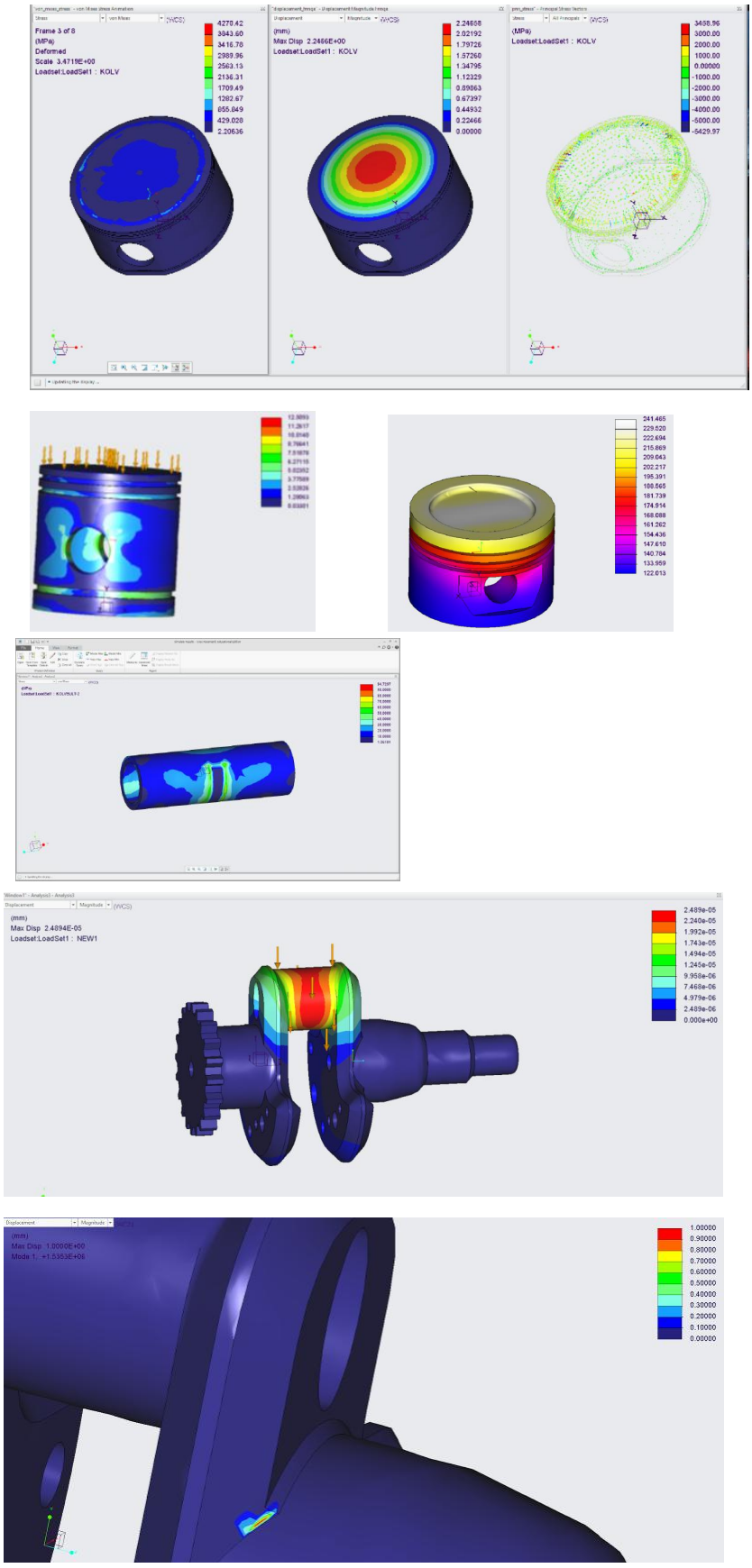

Figure 12. Thermo- mechanicals analyse of different components in general assembly.

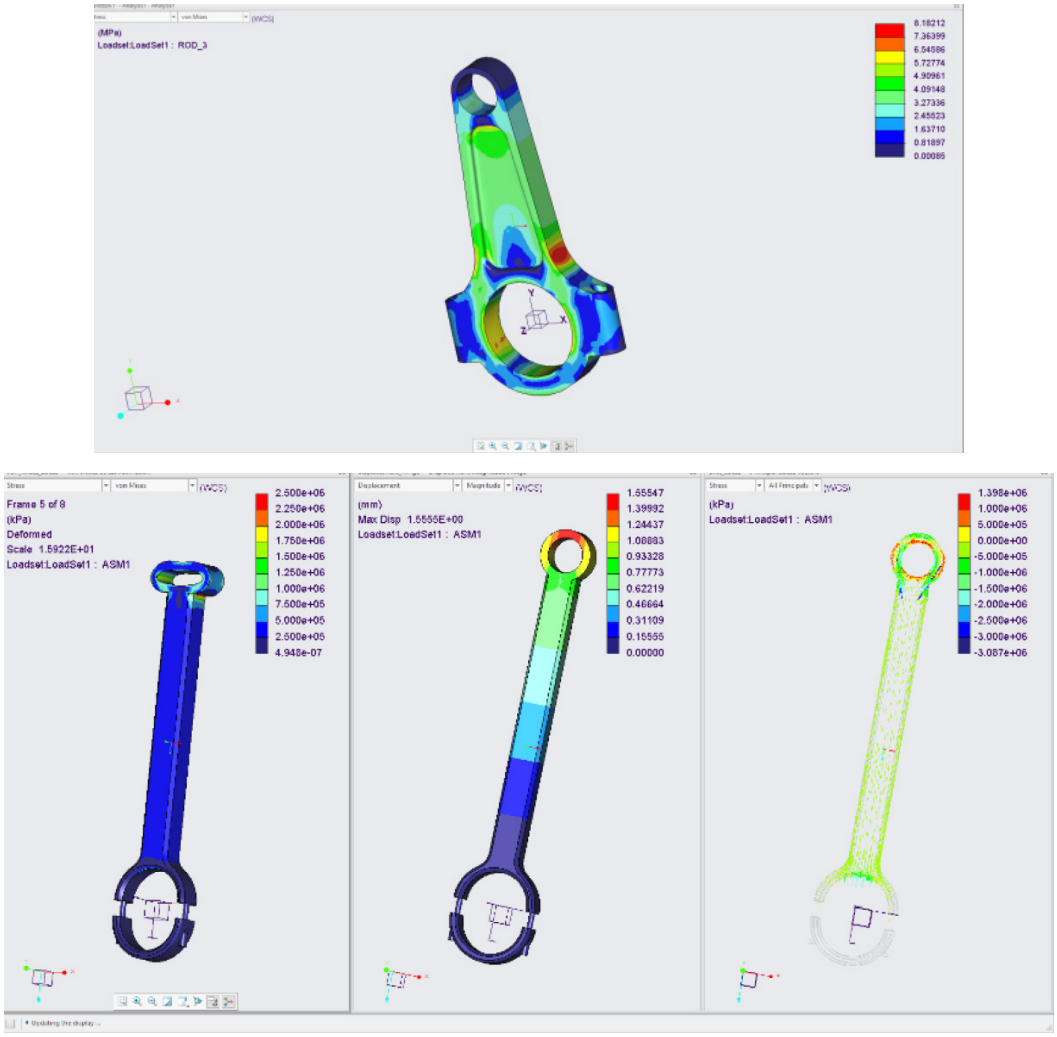

Figure 13. Thermo- mechanicals analyse of the connecting rod.

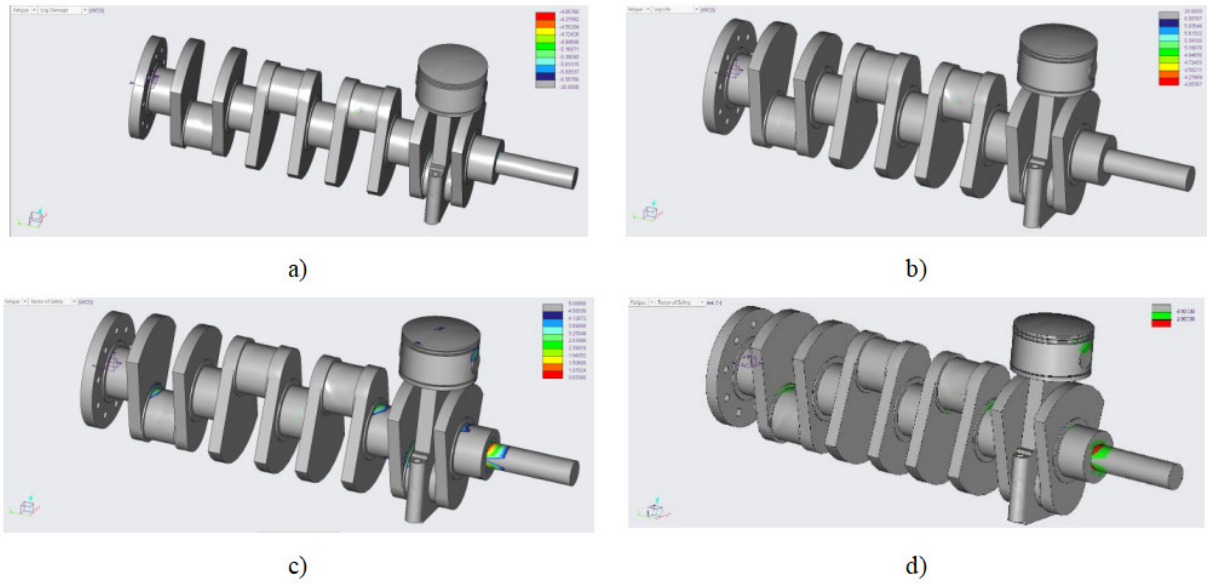

Figure 14. Fatigue analysis: (a) the logarithm of damage, (b) the logarithm of life of fatigue, (c) the factor of safety of fatigue, and (d) the confidence of the life

ance. Yellow means confidence of life varying from the cycle numbers of the optimal endurance to three times of that value. Also, green means any amount of nominal life cycles.

Figure 15 (a-e) shows the mode shapes 1 to 4, respectively. The buckling load factor is also available in Table 6. Regarding previous discussions and this table, mode shapes 1, 2, and 3 are greater than 1, so buckling does not occur. The last one is smaller than –1, in which buckling is avoided again.

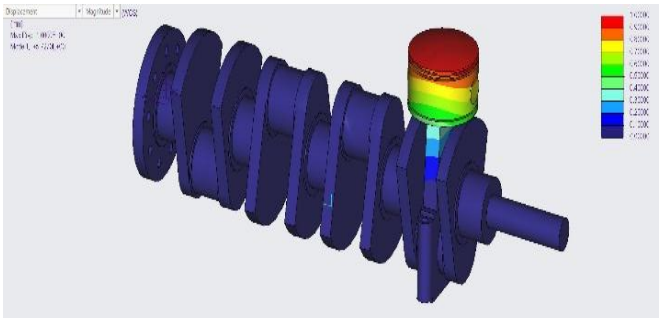

a)

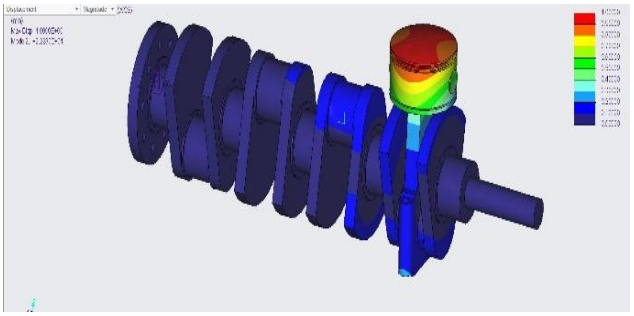

b)

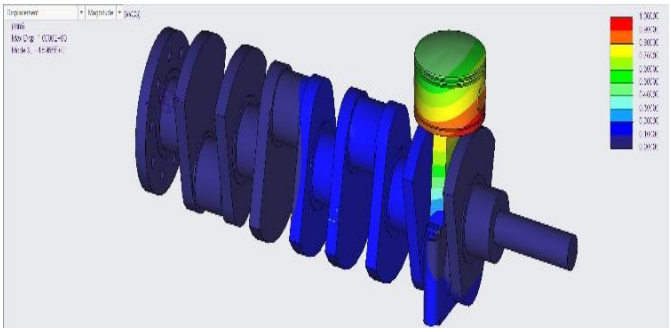

c)

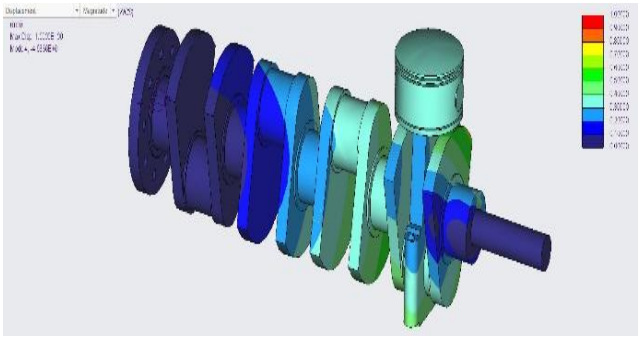

d)

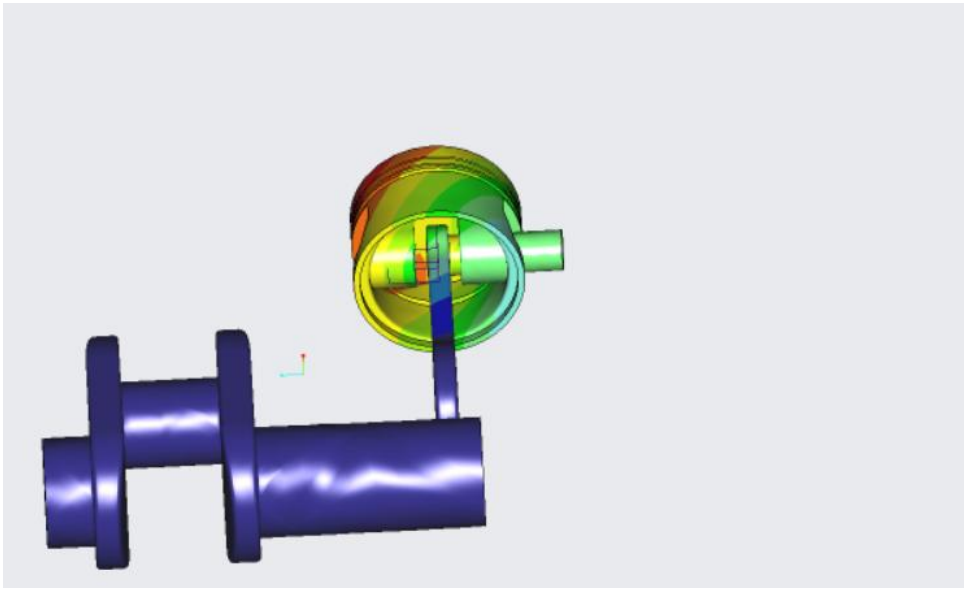

e)

Figure 15. Bucking analysis: (a) Displacement in buckling mode shape 1, (b) Displacement in buckling mode shape 2, (c) Displacement in buckling mode shape 3, and (d and e) Displacement in buckling mode shape 4.

Table 6. BLF and corresponding mode shapes

Mode Shape	Buckling Load Factor
1	5.72
2	22.27
3	45.96
4	–46.33

Figures 16 (a-e) show the displacement, maximum principle thermal stress, Von-mises thermal stress, and failure index thermal stress, respectively. Comparing the results from thermal stress and thermo-mechanical simulations, as Figure 16 shows, 0.12 mm is the maximum displacement caused by the thermal load. Considering Figure 9 from thermo-mechanical simulation, it is concluded that temperature has a 10% contribution in displacement. Also, comparing Figure 16a and Figure 16c shows that heating has participated 15% in stress. Finally, based on Figure 16d and e, failure in the thermo-mechanical case is caused 85% by mechanical load. Such a conclusion on the primacy of the mechanical load is reported [7] for thermo-mechanical loadings.

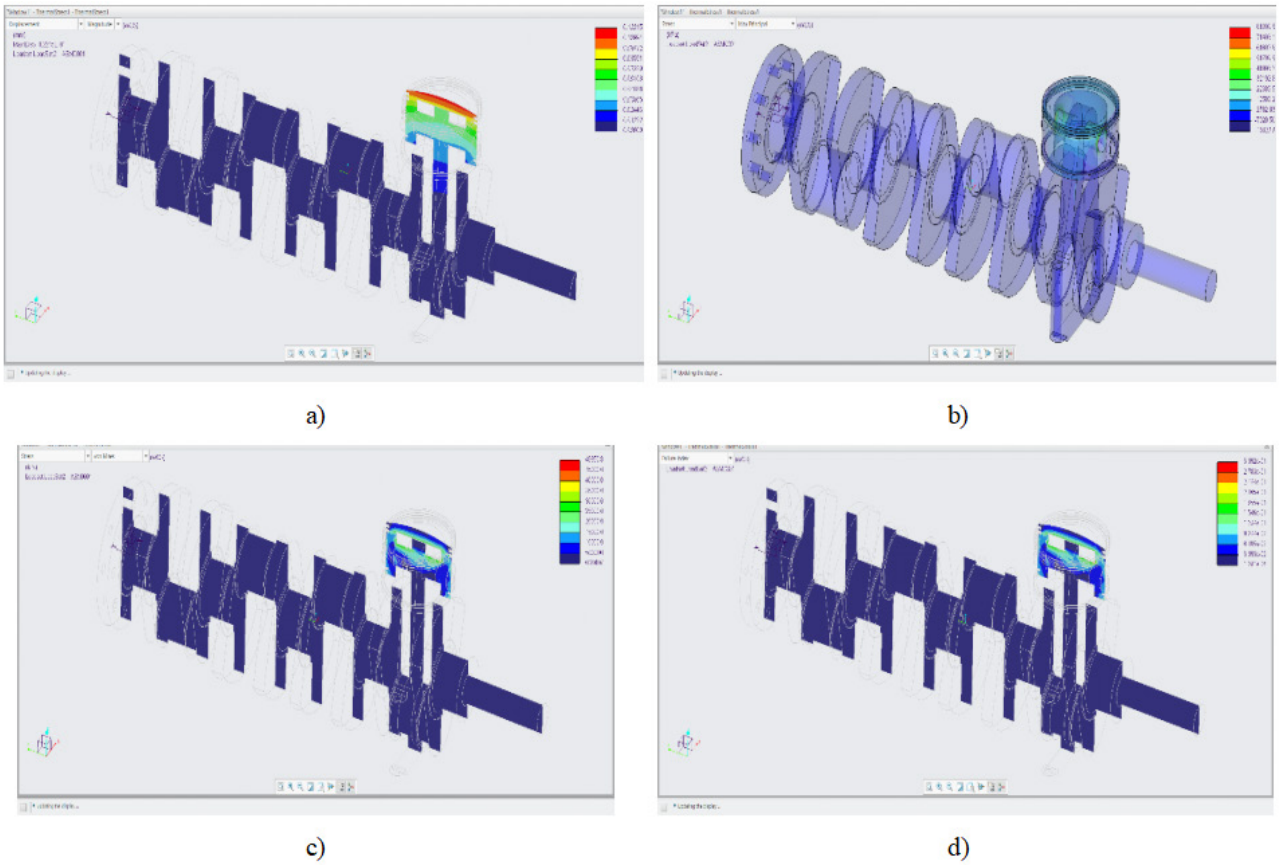

Figure 16. (a) Displacement thermal stress, (b) Max Principle thermal stress, (c) Von-mises thermal stress, and (d) failure index thermal stress.

5. Conclusions

In this study, a typical vehicle engine is simulated and analyzed under the thermal, mechanical, and thermo-mechanical loads. Also, the effects of different parameters on engine failure are investigated. The results showed that the maximum temperature is about 396 °K, the least temperature gradient is at the center of the pin which connects the piston to the connecting rod, most of the stress concentration is focused on the sharp corners, maximum displacement occurs just below the piston head, and the maximum failure index (minimum SF) is about 1.8. Besides, according to the dynamic response history, the maximum stress happened after approximately 0.001 seconds, the minimum and maximum values for the SF in fatigue analysis are 0.63 and 5, respectively, and the failure in the thermo-mechanical case is caused 85% by mechanical load rather than the thermal one.

It was seen that because of the greater impact of mechanical loads on the design process, mechanical forces and thermal stress effects on other parts should not be neglected. Expectedly, the sharp corners have more possibil-

ity to failure rather than round one. Therefore, these areas should be given more attention. In addition to reducing sharp corners as much as possible (e.g., more rounding of the connecting rod's radius [36]), design and manufacturing strategies such as shot peening should be used to prevent the accumulation of stress in critical areas, thereby increasing fatigue strength as well as preventing damage to a large extent. The results provide a basis for the theoretical analysis for the reliability of a typical vehicle engine.

Conflict of Interest

There is no conflict of interest.

References

[1] Hermawan, M.V., Anggono, A.D., Siswanto, W.A., et al., 2019. The Influence of Material Properties to the Stress Distribution on Piston, Connecting Rod and Crankshaft of Diesel Engine. International Journal of Mechanical & Mechatronics. 19(6), 13-26.

[2] Deulgaonkar, V.R., Ingolikar, N., Borkar, A., et al., 2021. Failure analysis of diesel engine piston in transport utility vehicles. Engineering Failure Analysis. 120, 105008.

[3] Xu, X.L., Yu, Zh.W., 2018. Failure analysis of a truck diesel engine crankshaft. Engineering Failure Analysis. 92, 84-94.

[4] Zhang, M.Q., Zhao, Ch., Yan, Zh.Q., et al., 2019. The Structure, Stress and Modal Analysis of 1.6-Liter Gasoline Engine Connecting Rod Based on Finite Element Analysis. IOP Conference Series: Materials Science and Engineering. 677(3), 032094.

[5] Viet Nguyen, D., Duy, V.N., 2018. Numerical analysis of the forces on the components of a direct diesel engine. Applied Sciences. 8(5), 761.

[6] Liu, X., Wang, Y., Liu, W., 2017. Finite element analysis of thermo-mechanical conditions inside the piston of a diesel engine. Applied Thermal Engineering. 119, 312-318.

[7] Qin, Zh.J., Li, Y.S., Yang, Zh.Zh., et al., 2019. Diesel engine piston thermo-mechanical coupling simulation and multidisciplinary design optimization. Case Studies in Thermal Engineering. 15, 100527.

[8] Gopi, E., Saleem, M., Chandan, S., et al., 2019. Thermal and static analysis of engine piston rings. International Journal of Ambient Energy. 1-5.

[9] Rajakumar, S., Karthiyaraj, M., 2020. A comparative study of structural and thermal analyses on piston materials. International Journal of Scientific Development and Research (IJSDR). 5(12).

[10] Strozzi, A., Baldini, A., Giacopini, M., et al., 2016. A repertoire of failures in connecting rods for internal combustion engines, and indications on traditional and advanced design methods. Engineering Failure Analysis. 60, 20-39.

[11] Anderson, A., Yukioka, M., 2012. Connecting rod buckling analysis using eigenvalue and explicit methods. No. 2012-32-0102. SAE Technical Paper.

[12] Muhammad, A., Shanono, I.H., 2019. Static analysis and optimization of a connecting rod. Journal of Engineering and Technological Sciences. 6(1), 24-40.

[13] Pani, A.R., Patel, R.K., Ghosh, G.K., 2020. Buckling analysis and material selection of connecting rod to avoid hydro-lock failure. Materials Today: Proceedings. 27, 2121-2126.

[14] Rezvani, M.A., Javanmardi, D., Mostaghim, P., 2018. Diagnosis of EMD645 diesel engine connection rod failure through modal testing and finite element modeling. Engineering Failure Analysis. 92, 50-60.

[15] Witek, L., Zelek, P., 2019. Stress and failure analysis of the connecting rod of diesel engine. Engineering Failure Analysis. 97, 374-382.

[16] Andoko, A., Nauri, I.M., Paryono, P., et al., 2020. Failure analysis on the connecting rod by finite element method. AIP Conference Proceedings. 2262(1), 040011.

[17] Rodrigues, A., Silva, R.L., Cruz, R., et al., 2011. Experimental and numerical modal analysis of 6 cylinders diesel crankshaft. No. 2011-36-0358. SAE Technical Paper.

[18] Ang, Y.Z., Pei, X.K., 2021. Study on Failure Analysis of Crankshaft Using Finite Element Analysis. MATEC Web of Conferences. 335, 03001. EDP Sciences.

[19] Kumar, M., Senthil, S.R., Suresh, M., 2014. Analysis of crankpin failure in a single cylinder engine. International Journal of Mechanical Engineering and Robotics Research. 3(4), 260.

[20] Sola, J.F., Alinejad, F., Rahimidehgolan, F., et al., 2019. Fatigue life assessment of crankshaft with increased horsepower. International Journal of Structural Integrity.

[21] Infante, V., Freitas, M., Fonte, M., 2019. Failure analysis of a crankshaft of a helicopter engine. Engineering Failure Analysis. 100, 49-59.

[22] Gomes, J., Gaivota, N., Rui, F.M., et al., 2018. Failure analysis of crankshafts used in maritime V12 diesel engines. Engineering Failure Analysis. 92, 466-479.

[23] Jiao, A.Y., Liu, B.H., Chen, X.M., et al., 2020. Fracture failure analysis of KL crankshaft. Engineering Failure Analysis. 112, 104498.

[24] Kurbet, S.N., Kuppast, V.V., Talikoti, B., 2020. Material testing and evaluation of crankshafts for structural analysis. Materials Today: Proceedings.

[25] Kumar, K.S., 2016. Design and Analysis of IC Engine Piston and Piston-Ring on Composite Material Using Creo and Ansys Software. Journal of Engineering and Science. 1(1), 39-51.

[26] Prasad, D.R., Naga, Ch.S., 2017. Design and Analysis of 150CC IC Engine Connecting Rod. International Journal of Scientific Engineering and Technology Research 6(17), 3397-3402.

[27] Bedse, U.A., 2016. Developing a GUI based Design Software in VB Environment to Integrate with CREO for Design and Modeling of CI Engine. International Journal of Latest Trends in Engineering and Technology (IJLTET). 6(4).

[28] Yang, J., Wang, Y., Xiao, M.W., 2011. Heat load analysis of piston based on the ANSYS. Advanced Materials Research. 199, 1192-1195.

[29] Citti, P., Giorgetti, A., Millefanti, U., 2018. Current challenges in material choice for high-performance engine crankshaft. Procedia Structural Integrity. 8, 486-500.

[30] Ellis, D.E., 1960. Mechanical properties of aluminum alloys at various temperature *S*. No. NAA-SR-Memo-5716. Atomics International. Division of North American Aviation, Inc., Canoga Park, California.

[31] Sirata, G.G., 2020. Fatigue Failure Analysis of Crankshafts-A Review. IJISET-International Journal of Innovative Science, Engineering & Technology. 7(5).

[32] Baumel Jr, A., Seeger, T., 1990. Materials data for cyclic loading. Supplement 1. Elsevier Science Publishers, P. O. Box 211, 1000 AE Amsterdam, The Netherlands.

[33] Korkmaz, S., 2010. Uniform material law: extension to high-strength steels: a methodology to predict fatigue life of high-strength steels. VDM.

[34] Zienkiewicz, O.C., Taylor, R.L., 1977. The Finite Element Method, Third editions.

[35] Jangam, S.P., Kumar, S., Maheshwari, S., 2018. Literature review on analysis of various components of IC engine. Materials Today: Proceedings. 5(9), 19027-19033.

[36] Rakic, S., Bugaric, U., Radisavljevic, I., et al., 2017. Failure analysis of a special vehicle engine connecting rod. Engineering Failure Analysis. 79, 98-109.